scientific reports

Check for updates

OPEN

Influence of parent vessel feature on the risk of internal carotid artery aneurysm rupture via computational method

Mehdi Fattahi[1,2], Seyyed Amirreza Abdollahi[3]✉, Ali Hosin Alibak[4], Saleh Hosseini[5]✉ & Phuyen Dang[1,2]

In this study, the role of sac section area and parent vessel diameter on the hemodynamic feature of the blood flow in selected internal carotid artery (ICA) aneurysms is comprehensively investigated. The changes of wall shear stress, pressure, and oscillatory shear index (OSI) of blood stream on the vessel for various aneurysms with coiling treatment. To attain hemodynamic factors, computational technique is used for the modeling of non-Newtonian transient blood flow inside the three different ICA aneurysms. Three different saccular models with various Parent vessel mean Diameter is investigated in this study. The achieved outcomes show that increasing the diameter of the parent vessel directly decreases the OSI value on the sac surface. In addition, the mean wall shear stress decreases with the increase of the parent vessel diameter.

Intracranial aneurysms are abnormal bulges or weak areas in the walls of blood vessels within the brain, particularly in the internal carotid artery (ICA). These aneurysms pose a significant risk of rupture, leading to potentially life-threatening hemorrhages. The rupture of an intracranial aneurysm remains a critical challenge in neurosurgery, and understanding the underlying hemodynamic factors contributing to aneurysm rupture is crucial for developing effective treatment strategies[1–3].

Hemodynamics, which refers to the study of blood flow patterns and forces within blood vessels, plays a vital role in the initiation, growth, and rupture of intracranial aneurysms. Various hemodynamic factors, such as wall shear stress, flow velocity, and pressure distribution, influence the structural integrity of an aneurysm. For instance, elevated wall shear stress and flow impingement on the aneurysm wall can lead to progressive weakening and eventual rupture[4,5]. There are several papers related to biomedical study via theoretical techniques[6–11]. The focused on different aspects of biomedical science[12–17].

To mitigate the risk of rupture, endovascular techniques, such as coiling, have emerged as an effective treatment option[18–20]. Coiling involves the placement of a small metal coil into the aneurysm sac to promote thrombosis and reduce blood flow into the aneurysm. However, the precise hemodynamic alterations induced by coiling and their impact on the risk of aneurysm rupture are not yet fully understood. There are various treatments for the problem related to human's health[21–27]

Computational fluid dynamics (CFD) has emerged as a valuable tool for investigating the hemodynamics of intracranial aneurysms and evaluating the effectiveness of treatment strategies. By simulating blood flow within patient-specific vascular geometries, CFD allows researchers to quantify key hemodynamic parameters and analyze their relationship with aneurysm rupture risk. This approach provides valuable insights into the complex flow patterns, wall shear stress distribution, and pressure gradients within the aneurysm[28–30].

The findings of this study have the potential to enhance our knowledge of the hemodynamic mechanisms underlying aneurysm rupture and the efficacy of coiling as a treatment strategy. Ultimately, this research may contribute to the development of improved clinical decision-making tools and personalized treatment approaches for patients with ICA aneurysms, with the goal of minimizing the risk of rupture and optimizing patient outcomes[31].

[1]Institute of Research and Development, Duy Tan University, Da Nang, Vietnam. [2]School of Engineering and Technology, Duy Tan University, Da Nang, Vietnam. [3]Faculty of Mechanical Engineering, University of Tabriz, Tabriz, Iran. [4]Petroleum Engineering Department, Faculty of Engineering, Soran University, Soran, Kurdistan Region 44008, Iraq. [5]Department of Chemical Engineering, University of Larestan, Larestan, Iran. ✉email: s.a_abdollahi@yahoo.com; saleh.o.hosseini95@gmail.com; sh850544@lar.ac.ir

Several key hemodynamic parameters are commonly studied in relation to aneurysm rupture risk[32,33]. These parameters provide insights into the flow patterns and forces acting on the aneurysm wall, which can play a crucial role in aneurysm initiation, growth, and rupture. Some of the key hemodynamic parameters will be explained. Wall Shear Stress (WSS) is the tangential force exerted by flowing blood on the vessel wall. Elevated WSS has been associated with increased aneurysm rupture risk. High WSS can lead to endothelial dysfunction, inflammation, and remodeling of the vessel wall, potentially weakening it over time. Flow velocity refers to the speed at which blood flows through the aneurysm and adjacent vessels. Disturbed flow patterns, characterized by high-velocity jets, vortices, and flow impingement on the aneurysm wall, have been linked to an increased risk of aneurysm rupture. Pressure distribution within the aneurysm sac and surrounding vessels can influence the mechanical stress on the aneurysm wall. High-pressure gradients and localized pressure peaks within the aneurysm may contribute to wall degeneration and rupture[34,35].

The complex flow patterns within the aneurysm, such as recirculation zones and flow impingement, are of interest in understanding the hemodynamics of aneurysms. Disturbed flow patterns can result in regions of low wall shear stress or high pressure, which may promote aneurysm growth and rupture. Energy loss quantifies the dissipation of kinetic energy within the aneurysm[36]. Higher energy loss has been associated with increased rupture risk, as it indicates inefficient flow patterns and flow disturbances that can weaken the aneurysm wall. Oscillatory Shear Index (OSI) measures the degree of oscillatory flow and changes in the direction of shear stress. High OSI values have been correlated with aneurysm initiation and progression, suggesting a potential role in rupture risk assessment. By studying these and other hemodynamic parameters, researchers can gain valuable insights into the complex interplay between blood flow dynamics and aneurysm rupture. Computational fluid dynamics (CFD) simulations and advanced imaging techniques play a crucial role in quantifying these parameters and investigating their relationship with aneurysm behavior, providing a foundation for improved risk prediction and treatment strategies.

In this study, we aim to explore the role of hemodynamic factors on the risk of rupture in ICA aneurysms and investigate how the coiling technique influences these factors using a computational fluid dynamics approach. By integrating patient-specific vascular geometries, physiological flow conditions, and accurate modeling of coiling procedures, we can gain a deeper understanding of the hemodynamic modifications induced by coiling and their implications for aneurysm rupture risk reduction.

Although several investigations have analyzed the aneurysm feature on the risk of bleeding, limited research has presented valuable information on the role of parent vessel mean diameter on the hemodynamic characteristics of blood flow inside the ICA aneurysms. This work tries to investigate the role of Parent vessel mean diameter on the hemodynamic factors related to the bleeding of the saccular ICA aneurysms. Computational fluid dynamic is used to visualize the blood stream inside real three-dimensional ICA aneurysms. Wall shear stress and OSI value in various stages of the cardiac cycle.

Governing equations and numerical method

For the selection of the ICA aneurysms, more than 100 aneurysms with different geometrical sizes are obtained from Aneurisk[37] and their geometrical features are compared based on the sac section area and parent mean diameter. It is confirming that all methods were carried out in accordance with relevant guidelines and regulations. Besides, all experimental protocols were approved by of the Ca' Granda Niguarda Hospital and it is confirmed that informed consent was obtained from all subjects and/or their legal guardian(s).

Among these cases, three cases are chosen (Fig. 1), and details of the selected aneurysms are presented in Table 1. As presented in the table, three female patients with different sizes of sac section area and parent vessel mean diameter. The HCT of the blood is 0.4 since the patients are female. Since the aneurysms are filled with coiling, it is assumed that the porous media is applied in the saccular domain. In Table 2, the facts of applied porosity and viscous residence (permeability) are presented.

The study of the blood stream moves inside the parent vessel and saccular aneurysm requires specific considerations. Transient Navier Stokes equations are used for the modeling of the blood flow inside the aneurysms[38–40]. One-way FSI approach is considered for the interaction of the vessel and aneurysm wall with blood flow[30,41]. Due to non-Newtonian blood characteristics, the Casson model is conventionally applied to calculate the viscosity of the blood within the vessel[32,42]. The flow is assumed laminar since the velocity of the blood is not high. ANSYS-FLUENT is used for the modeling of the blood flow within saccular aneurysms[43]. This software used for different engineering applications[44–49]

Since the blood flow inside the aneurysms and parent vessel is transient, mass flow rate and pressure outlet are applied at the inlet and outlet, respectively. Figure 2 plots the applied mass and pressure profile at the inlet and outlet, respectively. The maximum flow rate of the blood is at peak systolic and the end of the cardiac cycle is named early diastolic. In the former, wall shear stress is reported while the OSI index is reported at the end of the cardiac cycle. Figure 3 illustrates the produced grid for the chosen cases with a close-up view. As shown in Fig. 3, the hexagonal uniform structured grids are used for the selected saccular and parent vessels. The number of produced grids for these models is between 840,000 and 1,100,000 cells.

Results and discussion

The hemodynamic results of the simulation of the blood inside the selected aneurysm are presented in Table 3. The mean and minimum WSS, mean OSI, mean wall pressure, and mean blood velocity inside the aneurysm are presented in Table 3. Full contour and plots are presented subsequently to explain the main effective terms on the hemodynamic factors.

Figure 4a plots the variation of the minimum wall shear stress of selected aneurysms in different sac section areas. The archived results indicate that the minimum wall shear stress is decreased by about 50% by increasing

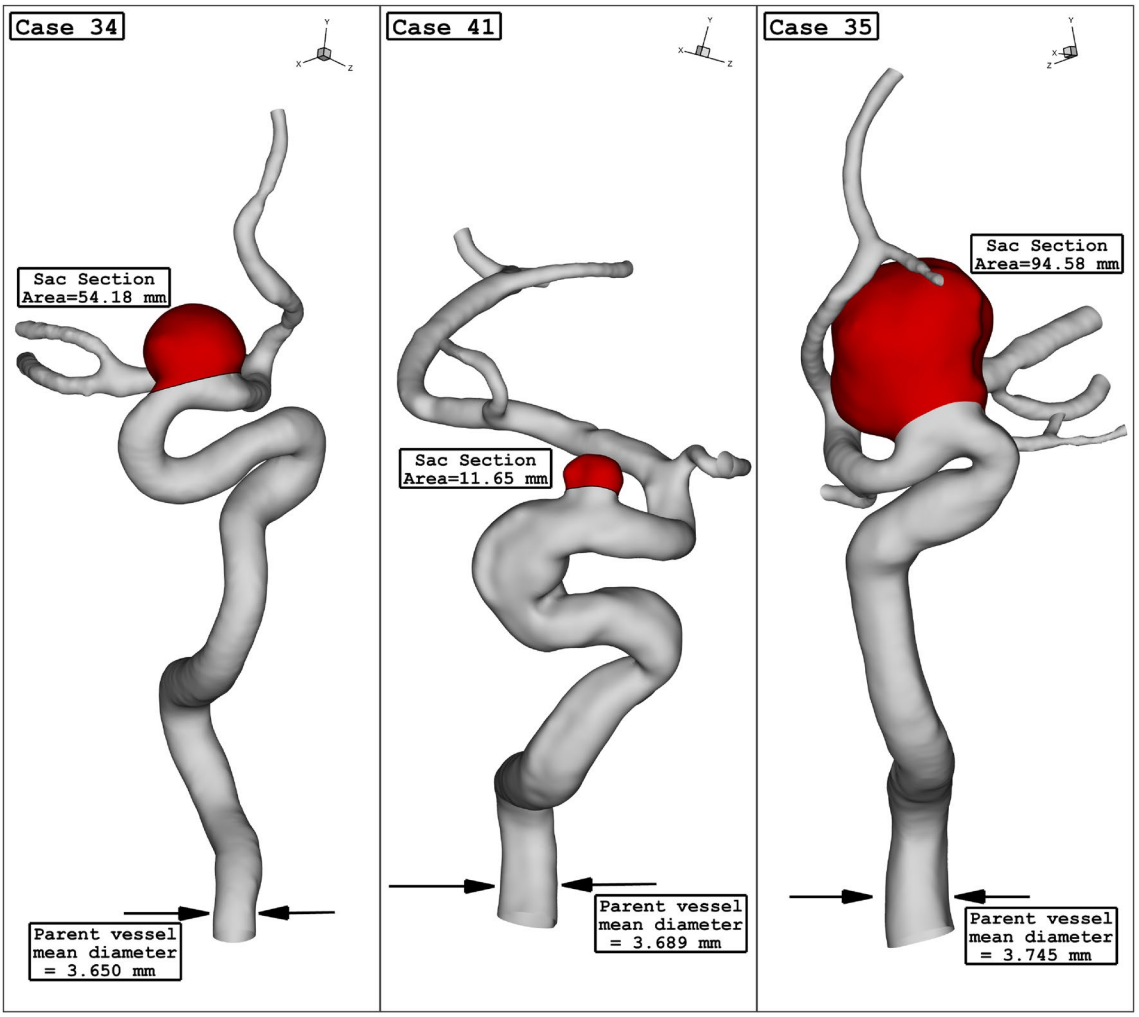

Figure 1. ICA aneurysm geometry of 3 different cases.

Case ID	Parent vessel mean diameter (mm)	Sac section area (mm^2)	Sex
34	3.650	54.18	Female (HCT = 0.40)
41	3.689	11.65	Female (HCT = 0.40)
35	3.745	94.58	Female (HCT = 0.40)

Table 1. geometrical details of chosen ICA sac.

HCT	Porosity	Viscous resistance (m^2/l)
0.4	0.844	16,958,264.02

Table 2. Coiling characteristic inside aneurysm sac.

of the sac section area from 11 to 94 mm^2. Considerable reduction in this change may related to the high increase of incoming blood flow by increasing of sac section area. In Fig. 4b, the effects of vessel diameter on the mean wall shear stress are disclosed. As the mean diameter of the parent vessel increases slightly, the value of mean wall shear stress drops from 8 pas to 2 Pa. Figure 5 illustrates the contour of WSS of different cases at peak systolic. Variation of the WSS indicates that the value of this index is higher near the neck area where incoming blood flow enters the sac and returns to the parent vessel. It is also perceived that the WSS in the dome section is not high.

The variation of the mean sac wall pressure of the selected aneurysm in a diverse range of parent vessel means diameter at peak systolic stage is demonstrated in Fig. 6. It is observed that pressure changes happen due to the changes in the parent vessel's mean diameter. As the size of the parent vessel diameter is increased, the mean

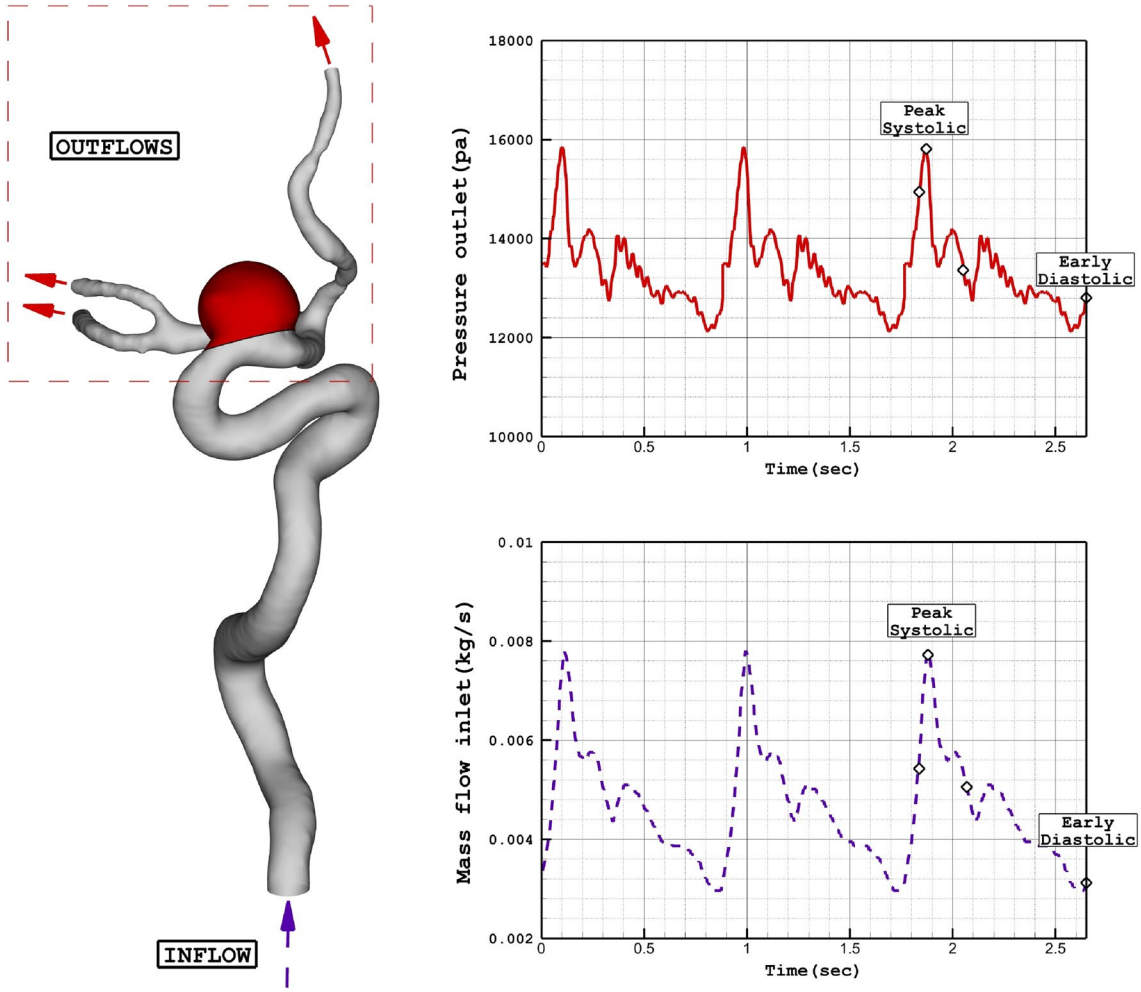

Figure 2. Applied mass and pressure profile at inlet and outlets.

pressure of the blood flow inside the sac is decreased. Figure 7 illustrates the contour of the pressure on the sac surface at peak systolic. The variation of the pressure shows that the maximum pressure on the sac wall occurs in the region where the incoming blood contact with the wall of the aneurysm.

The variation of the mean oscillatory shear index (OSI) at early diastolic for various parent vessel mean diameters is demonstrated in Fig. 8. The OSI value is decreased as the parent vessel diameter is increased. In case 35, the mean value of OSI is approximately zero which means that the changes in OSI in this model are considerably lower than other models. Figure 9 confirms that the range of OSI on the sac surface of case 35 is lower than in the other two cases. Indeed, this model has a larger sac section area than others and its parent vessel diameter is also more than the other two cases.

Figure 10 displays the effects of the parent vessel's mean diameter on the mean sac velocity inside the sac domain of the chosen cases. For case 34, the changes in the mean sac velocity have no meaningful connection to the parent vessel's mean diameter. Figure 11 demonstrates the streamline pattern inside the aneurysms and streamlines are colored by the velocity magnitude at peak systolic. The streamline indicates that the velocity of the blood inside the sac domain is lower than the main parent vessel. To demonstrate the blood flow structure, Fig. 12 displays the iso-velocity of the blood in the sac section which is filled by the coiling porosity. The blood velocity feature indicates the main shape of flow when a fraction of the domain is filled by the coil.

Conclusion

The present study investigates the influence of sac section area and parent vessel diameter on the hemodynamic feature of the blood flow in selected aneurysms. Computational fluid dynamic is applied for the modeling of the transient blood stream in the cardiac cycle. The selected aneurysms are treated and filled by the porous media. The variation of the mean OSI shows that increasing the diameter of the parent vessel directly decreases the OSI value on the sac surface. In addition, the mean WSS decreases with the increase of the parent vessel diameter.

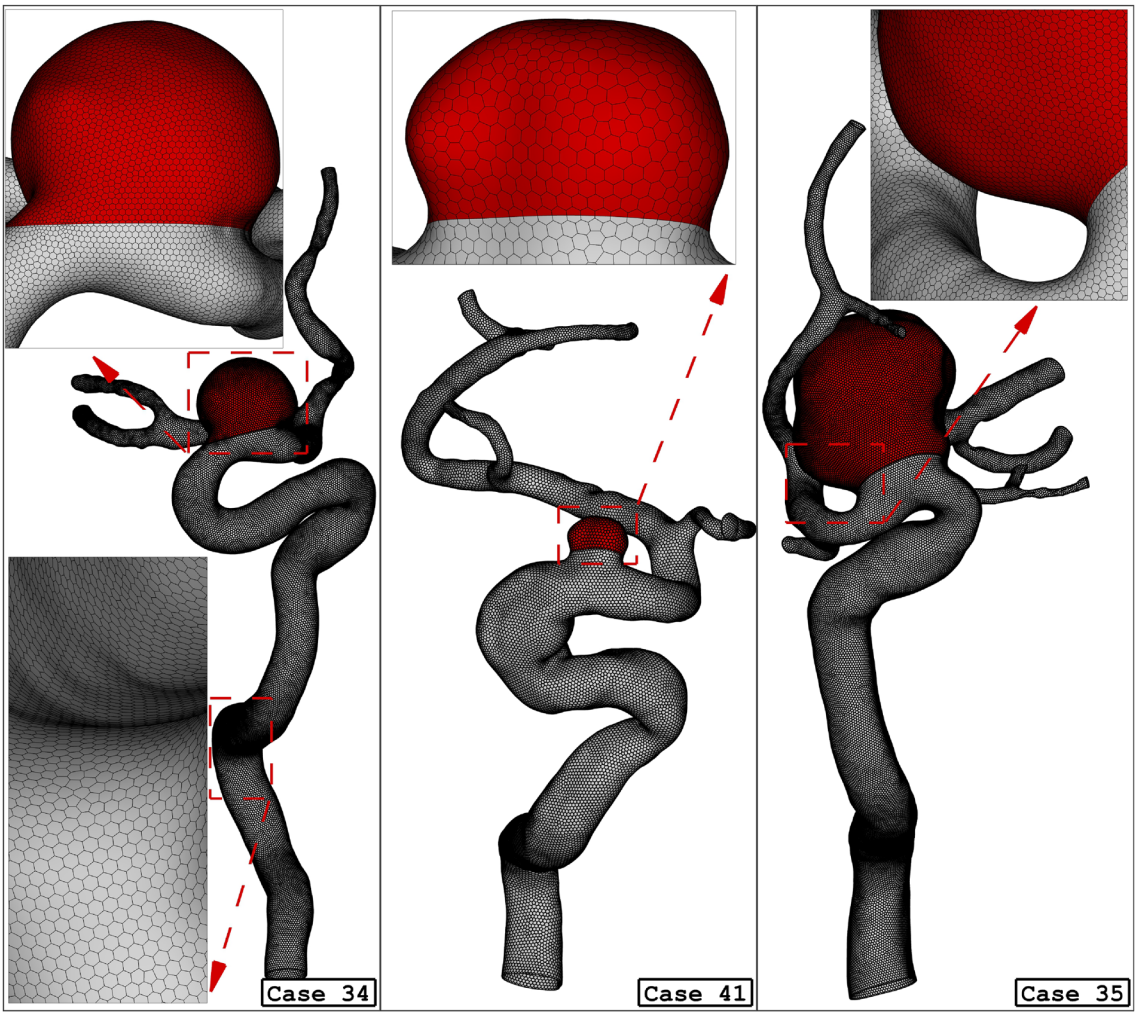

Figure 3. Grid generation for 3 different ICA cases.

	Parent vessel mean diameter (mm)	Sac section area (mm^2)	WSS_mean (Pa)	WSS_min (Pa)	OSI_mean	Wall pressure_mean (Pa)	Aneurysm velocity_mean (m/s)
Case 34	3.650	54.18	8.146665	0.130785	0.02603191	25,071.71	0.4034861
Case 41	3.689	11.65	4.200369	0.155615	0.01506075	24,503.94	0.1524694
Case 35	3.745	94.58	2.143452	0.075405	5.64e−5	20,665.31	0.1365955

Table 3. Details of hemodynamic analyses.

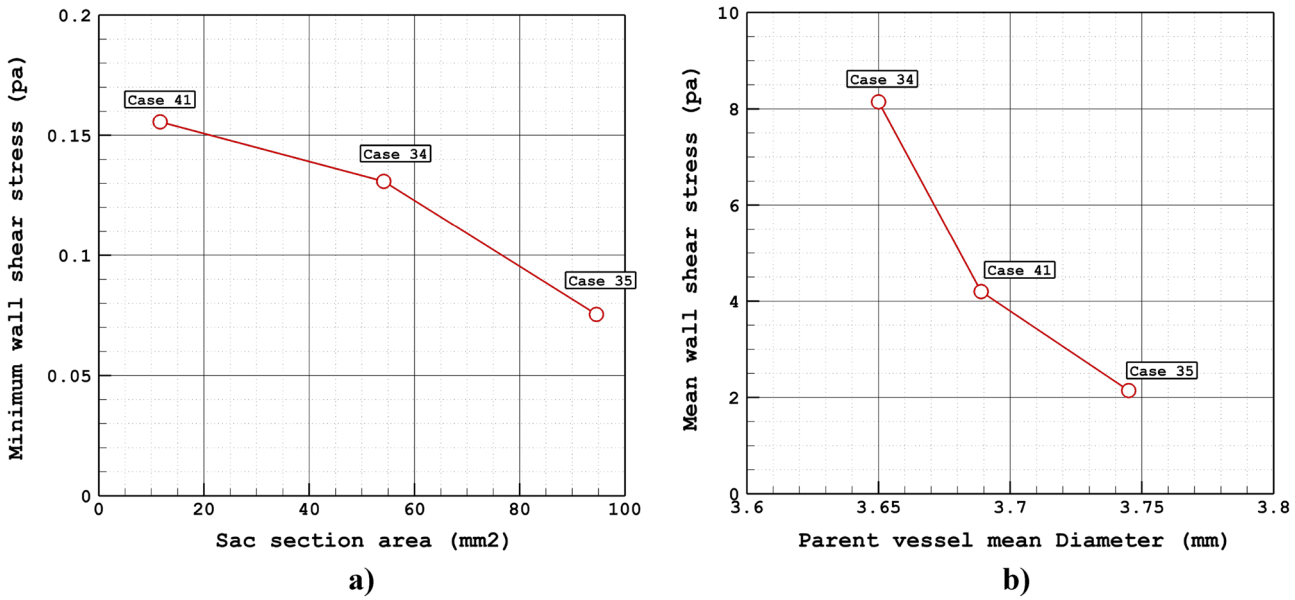

Figure 4. (**a**) Minimum, (**b**) mean wall shear stress vs sac section are at peak systolic.

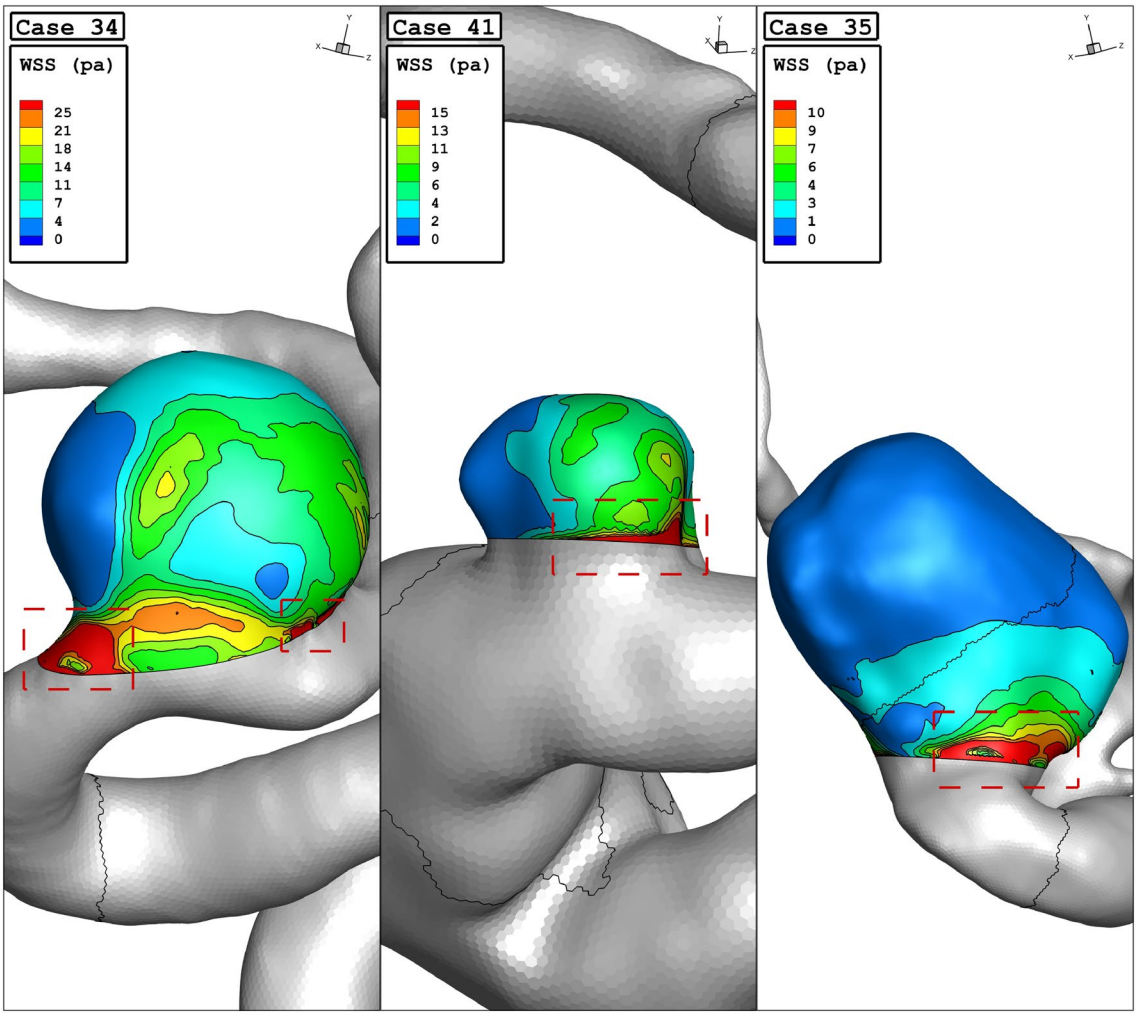

Figure 5. WSS contours (peak systolic) in different cases.

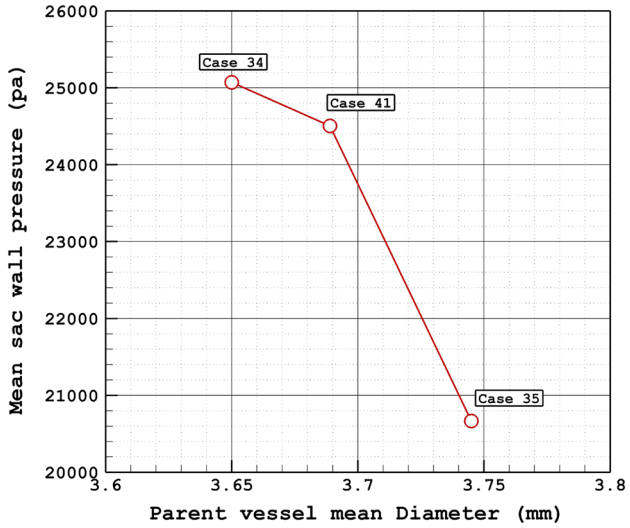

Figure 6. Mean wall pressure vs parent vessel mean diameter at peak systolic.

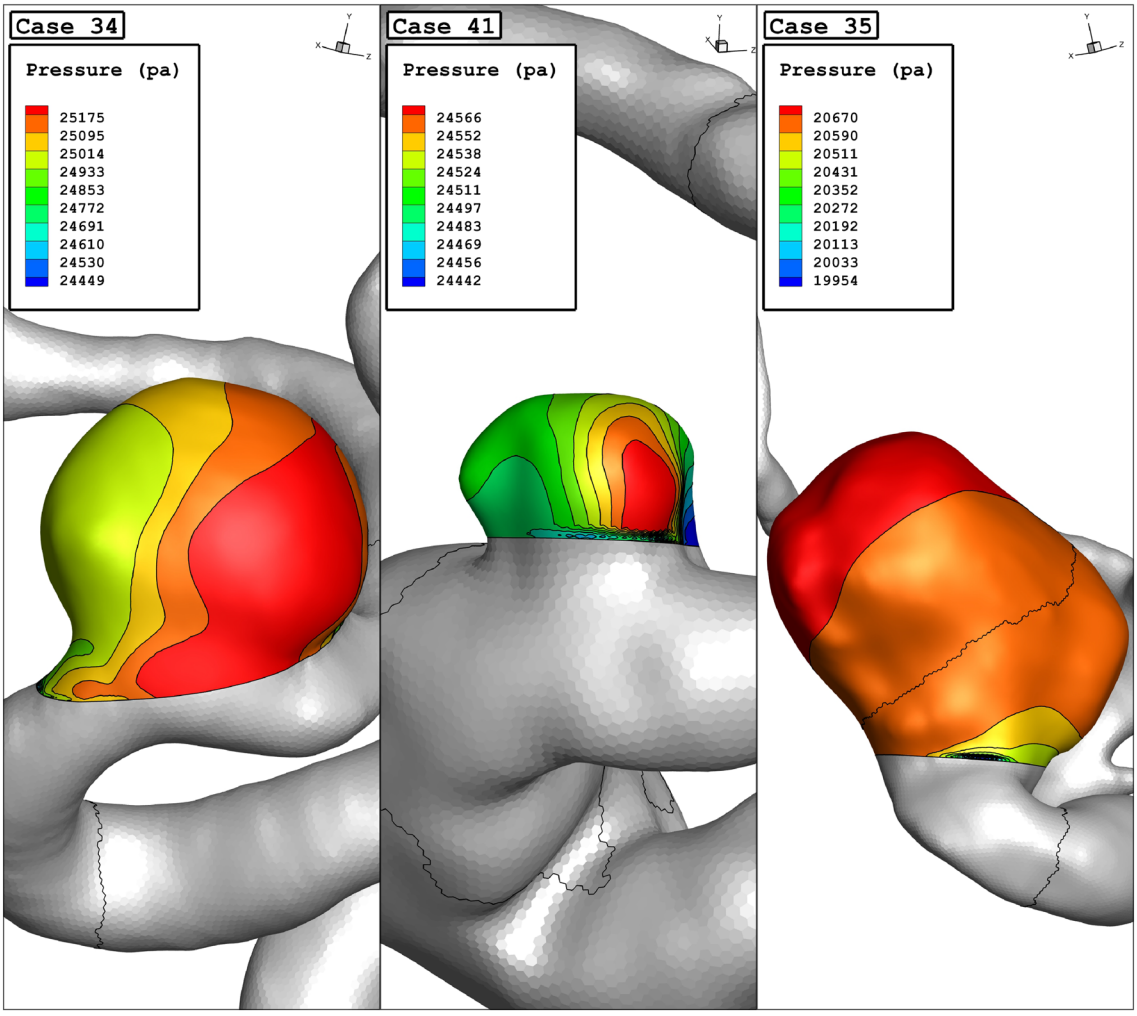

Figure 7. Wall pressure contours (peak systolic) in different cases.

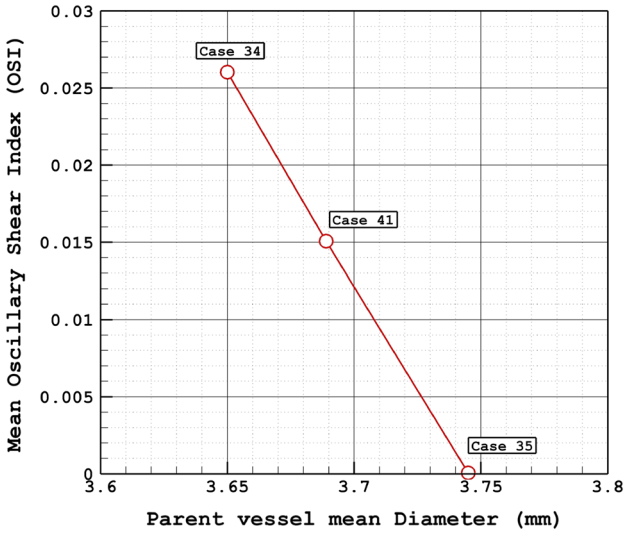

Figure 8. Mean OSI vs parent vessel mean diameter at early diastolic.

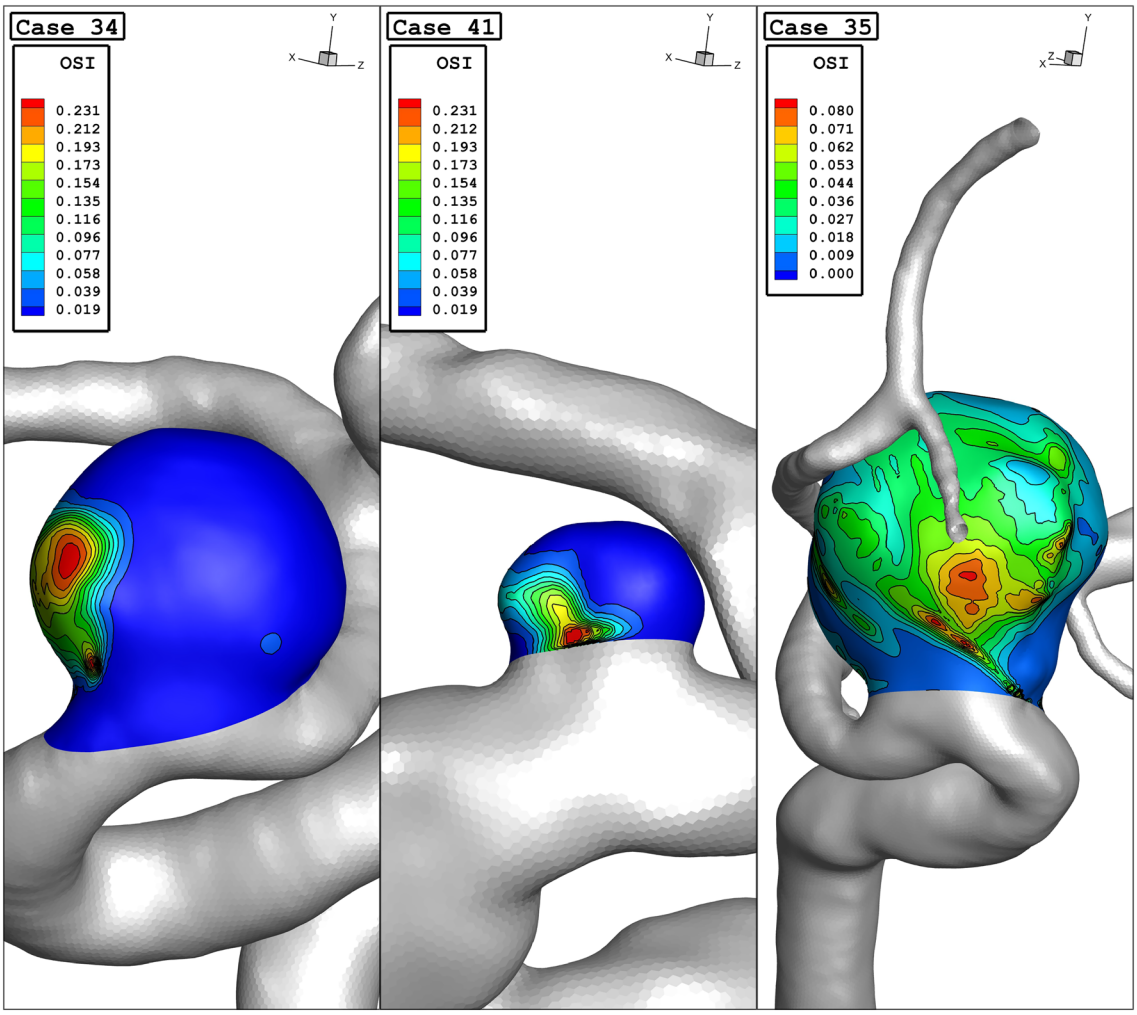

Figure 9. OSI contours (early diastolic) in different cases.

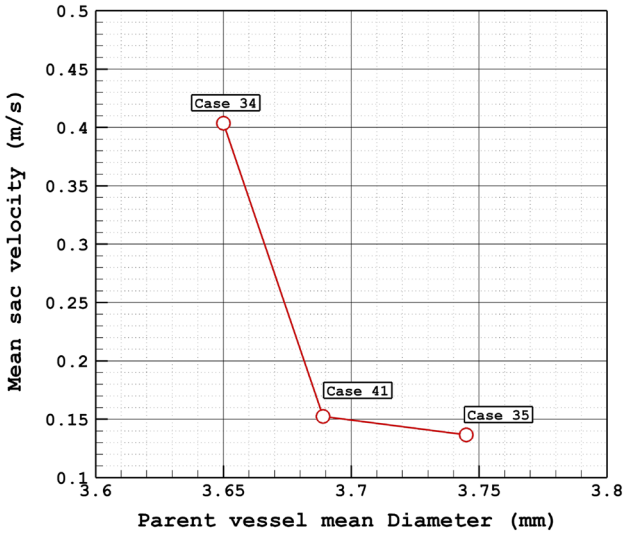

Figure 10. Mean sac velocity vs parent vessel mean diameter at peak systolic.

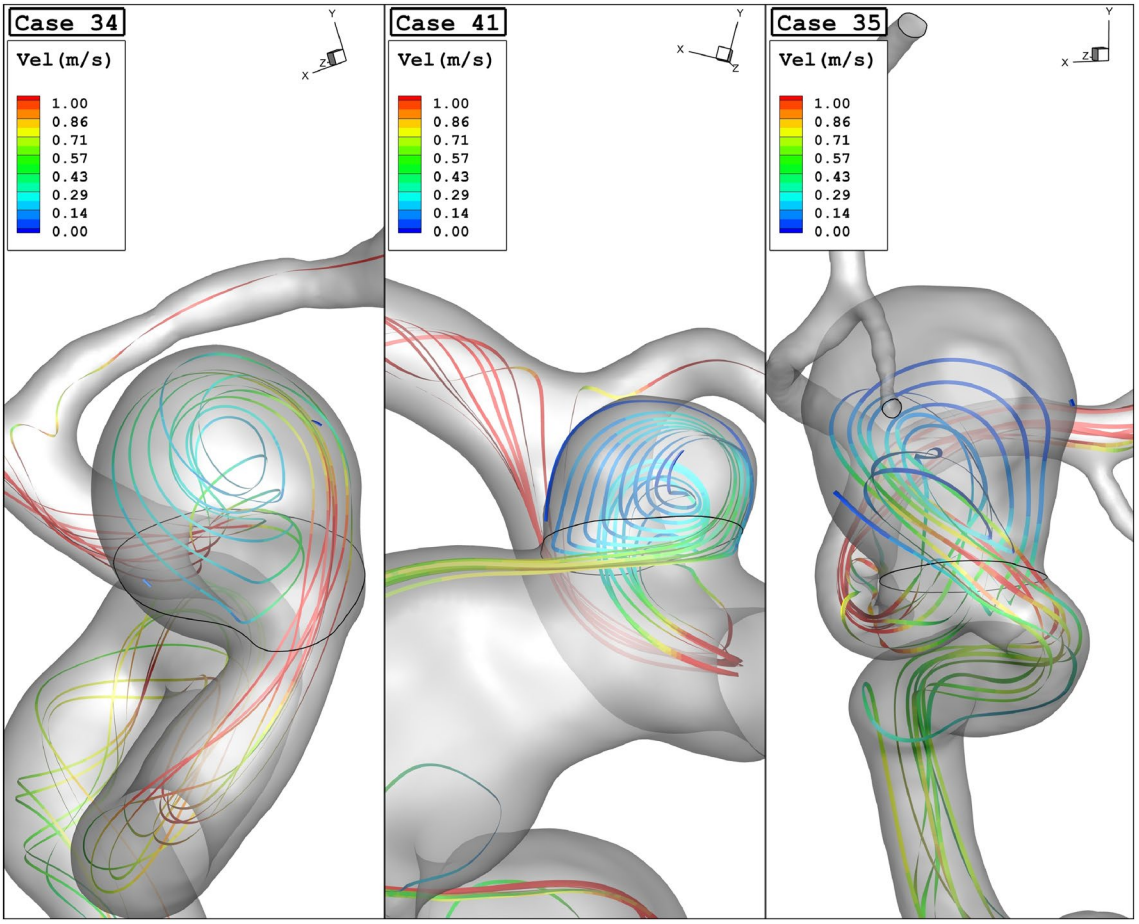

Figure 11. Streamlines (velocity at peak systolic) in different cases.

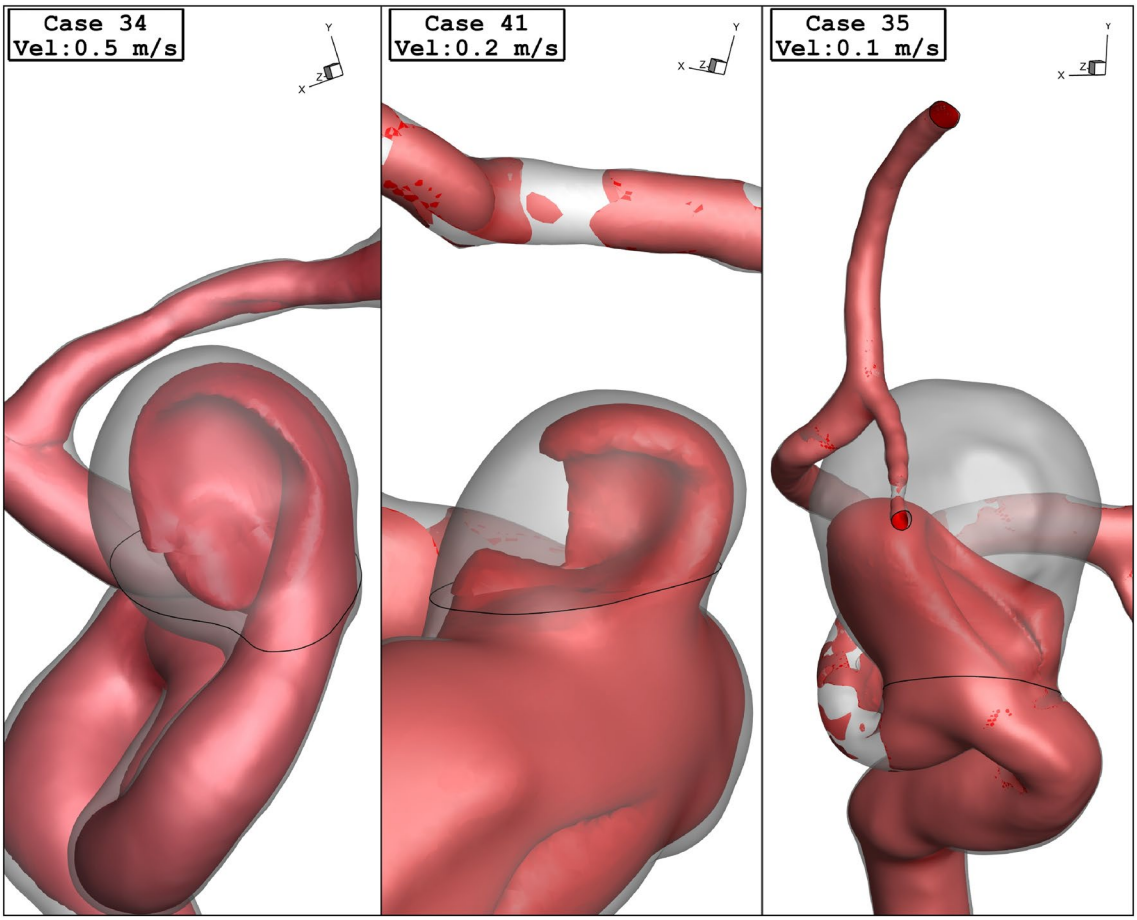

Figure 12. Iso-Surface (velocity at peak systolic) in different cases.

Data availability

All data generated or analysed during this study are included in this published article.

Received: 5 November 2023; Accepted: 20 November 2023
Published online: 23 November 2023

References

1. Poueinak, M. M., Abdollahi, S. A., Alizadeh, A., Youshanlui, M. A., Zekri, H. & Gerdroodbary, M. B. Computational study of blood hemodynamic in ICA aneurysm with coiling embolism. *Int. J. Mod. Phys. C* **34**(6), 2350138 (2023). https://doi.org/10.1142/S0129183123501383.
2. Sabernaeemi, A. *et al.* Influence of stent-induced vessel deformation on hemodynamic feature of bloodstream inside ICA aneurysms. *Biomech. Model Mechanobiol.* https://doi.org/10.1007/s10237-023-01710-9 (2023).
3. Hariri, S., Poueinak, M.M., Hassanvand, A., Gerdroodbary, M. B. & Faraji, M. Effects of blood hematocrit on performance of endovascular coiling for treatment of middle cerebral artery (MCA) aneurysms: Computational study. *Interdiscip. Neurosurg* **32**, 101729 (2023).
4. Rostamian, A., Fallah, K., Rostamiyan, Y. & Alinejad, J. Application of computational fluid dynamics for detection of high risk region in middle cerebral artery (MCA) aneurysm. *Int J. Mod. Phys. C* 2350019 (2022).
5. Shen, Xiao-Yong, M. Barzegar Gerdroodbary, Amin Poozesh, Amir Musa Abazari, and S. Misagh Imani. "Effects of blood flow characteristics on rupture of cerebral aneurysm: Computational study." *International Journal of Modern Physics C* 32, no. 11 (2021): 2150143.
6. Zhang, Z., Wang, L., Zheng, W. & Yin, L. Endoscope image mosaic based on pyramid ORB. *Biomed. Signal Process. Control* **71**, 103261. https://doi.org/10.1016/j.bspc.2021.103261 (2022).
7. Liu, Y., Tian, J., Hu, R., Yang, B. & Liu, S. Improved feature point pair purification algorithm based on SIFT during endoscope image stitching. *Front. Neurorobot.* https://doi.org/10.3389/fnbot.2022.840594 (2022).
8. Li, H., Peng, R. & Wang, Z. On a diffusive susceptible-infected-susceptible epidemic model with mass action mechanism and birth-death effect: Analysis, simulations, and comparison with other mechanisms. *SIAM J. Appl. Math.* **78**(4), 2129–2153. https://doi.org/10.1137/18M1167863 (2018).
9. Jin, H. & Wang, Z. Boundedness, blowup and critical mass phenomenon in competing chemotaxis. *J. Differ. Equ.* **260**(1), 162–196. https://doi.org/10.1016/j.jde.2015.08.040 (2016).
10. Shan, Y., Wang, H., Yang, Y., Wang, J. & Zhao, W. Evidence of a large current of transcranial alternating current stimulation directly to deep brain regions. *Mol. Psychiatry* https://doi.org/10.1038/s41380-023-02150-8 (2023).
11. Lu, S. & YangYang, J. B. Analysis and design of surgical instrument localization algorithm. *Comput. Model. Eng. Sci.* **137**(1), 669–685. https://doi.org/10.32604/cmes.2023.027417 (2023).

12. Ye, X., Wang, J., Qiu, W., Chen, Y., & Shen, L. Excessive gliosis after vitrectomy for the highly myopic macular hole: A spectral domain optical coherence tomography study. *Retina* **43**(2) (2023). https://doi.org/10.1097/IAE.0000000000003657.
13. Gao, Z., Pan, X., Shao, J., Jiang, X., Su, Z., Jin, K. & Ye, J. Automatic interpretation and clinical evaluation for fundus fluorescein angiography images of diabetic retinopathy patients by deep learning. *Br. J. Ophthalmol.* 2022-321472 (2022). https://doi.org/10.1136/bjo-2022-321472.
14. Zhao, J., Zhang, Q., Cheng, W., Dai, Q. & Wei, Z. Heart–gut microbiota communication determines the severity of cardiac injury after myocardial ischaemia/reperfusion. *Cardiovasc. Res.* **119**(6), 1390–1402. https://doi.org/10.1093/cvr/cvad023 (2023).
15. Chen, Y., Chen, L. & Zhou, Q. Genetic association between eNOS gene polymorphisms and risk of carotid atherosclerosis A meta-analysis. *Herz* **46**(2), 253–264. https://doi.org/10.1007/s00059-020-04995-z (2021).
16. Huang, A. & Zhou, W. Mn-based cGAS-STING activation for tumor therapy. *Chin. J. Cancer Res.* **35**(1), 19–43. https://doi.org/10.21147/j.issn.1000-9604.2023.01.04 (2023).
17. Wang, Y. *et al.* Rhubarb attenuates blood-brain barrier disruption via increased zonula occludens-1 expression in a rat model of intracerebral hemorrhage. *Exp. Ther. Med.* **12**(1), 250–256. https://doi.org/10.3892/etm.2016.3330 (2016).
18. Hassan, T. *et al.* Computational replicas: Anatomic reconstructions of cerebral vessels as volume numerical grids at three-dimensional angiography. *Am. J. Neuroradiol.* **25**, 1356–1365 (2004).
19. Tateshima, S., Vinuela, F., Villablanca, J.P., Murayama, Y., Morino, T. & Nomura, K. *et al.* Three-dimensional blood flow analysis in a wide necked internal carotid artery-ophthalmic artery aneurysm. *J. Neurosurg.* **99**, 526–533 (2003).
20. Jou, L. D. *et al.* Correlation between lumenal geometry changes and hemodynamics in fusiform intracranial aneurysms. *AJNR Am. J. Neuroradiol.* **26**, 2357–2363 (2005).
21. Mao, X. *et al.* Tissue resident memory T cells are enriched and dysfunctional in effusion of patients with malignant tumor. *J. Cancer* **14**(7), 1223–1231. https://doi.org/10.7150/jca.83615 (2023).
22. Liang, X. *et al.* Comparative study of microvascular structural changes in the gestational diabetic placenta. *Diabetes Vasc. Dis.Res.* **20**(3), 1497016315. https://doi.org/10.1177/14791641231173627 (2023).
23. Bing, P., Liu, Y., Liu, W., Zhou, J. & Zhu, L. Electrocardiogram classification using TSST-based spectrogram and ConViT. *Front. Cardiovasc. Med.* **9** (2022). https://doi.org/10.3389/fcvm.2022.983543.
24. Gao, X., Cai, X., Yang, Y., Zhou, Y., & Zhu, W. Diagnostic accuracy of the HAS-BLED bleeding score in VKA- or DOAC-treated patients with atrial fibrillation: A systematic review and meta-analysis. *Front. Cardiovasc. Med.* **8** (2021). https://doi.org/10.3389/fcvm.2021.757087.
25. Huang, H. *et al.* The behavior between fluid and structure from coupling system of bile, bile duct, and polydioxanone biliary stent: A numerical method. *Med. Eng. Phys.* **113**, 103966. https://doi.org/10.1016/j.medengphy.2023.103966 (2023).
26. Liu, H., Kong, L., Sun, Q. & Ma, X. The effects of mindfulness-based interventions on nurses' anxiety and depression: A meta-analysis. *Nurs. Open* **10**(6), 3622–3634. https://doi.org/10.1002/nop2.1610 (2023).
27. Zhou, L., Zhang, Q., Deng, H., Ou, S. & LiangZhou, T. J. The SNHG1-centered ceRNA network regulates cell cycle and is a potential prognostic biomarker for hepatocellular carcinoma. *Tohoku J. Exp. Med.* **258**(4), 265–276. https://doi.org/10.1620/tjem.2022.J083 (2022).
28. Shen, X.-Y., Barzegar Gerdroodbary, M., Abazari, A.M. & Moradi, R. Computational study of blood flow characteristics on formation of the aneurysm in internal carotid artery. *Eur. Phys. J. Plus* **136**(5), 541 (2021).
29. Shen, X.-Y., Xu, H.-Q., Barzegar Gerdroodbary, M., Valiallah Mousavi, S., Abazari, A.M. & Misagh Imani, S. Numerical simulation of blood flow effects on rupture of aneurysm in middle cerebral artery. *Int. J. Mod. Phys. C* **33**(03), 2250030 (2022).
30. Fung, Y. C. *Biomechanics: Mechanical Properties of Living Tissues* 2nd edn. (Springer, 1993).
31. Salavatidezfouli, S., Alizadeh, A., Barzegar Gerdroodbary, M., Sabernaeemi, A., Abazari, A. M. & Sheidani, A. Investigation of the stent induced deformation on hemodynamic of internal carotid aneurysms by computational fluid dynamics. *Sci. Rep.* **13**(1), 7155 (2023).
32. Sadeh, A. *et al.* Computational study of blood flow inside MCA aneurysm with/without endovascular coiling. *Sci. Rep.* **13**, 4560. https://doi.org/10.1038/s41598-023-31522-x (2023).
33. Jin, Z.-H., Barzegar Gerdroodbary, M., Valipour, P., Faraji, M. & Abu-Hamdeh, N.H. CFD investigations of the blood hemodynamic inside internal cerebral aneurysm (ICA) in the existence of coiling embolism. *Alex. Eng. J.* (2023). https://doi.org/10.1016/j.aej.2022.10.070.
34. Sheidani, A. *et al.* Influence of the coiling porosity on the risk reduction of the cerebral aneurysm rupture: Computational study. *Sci. Rep.* **12**, 19082 (2022).
35. Boccadifuoco, A., Mariotti, A., Celi, S., Martini, N. & Salvetti, M. V. Impact of uncertainties in outflow boundary conditions on the predictions of hemodynamic simulations of ascending thoracic aortic aneurysms. *Comput. Fluids* **165**, 96–115 (2018).
36. Mitsos, A.P., Kakalis, N.M.P., Ventikos, Y.P. & Byrne, J.V. Haemodynamic simulation of aneurysm coiling in an anatomically accurate computational fluid dynamics model. *Neuroradiology* **50**(4), 341–347 (2008).
37. AneuriskWeb project website. http://ecm2.mathcs.emory.edu/aneuriskweb. (Emory University, Department of Math & CS, 2012).
38. Jiang, H., Lu, Z., Barzegar Gerdroodbary, M., Sabernaeemi, A. & Salavatidezfouli, S. The influence of sac centreline on saccular aneurysm rupture: Computational study. *Sci. Rep. 13*(1), 11288 (2023).
39. Othman, G. Q., Saeed, R. S., Kadir, D. H., & Taher, H. J. Relation of angiography to hematological, hormonal and some biochemical variables in coronary artery bypass graft patients. *J. Phys. Conf. Ser.* (IOP Publishing) **1294**(6), 062110 (2019).
40. Hu, H., Luo, P., Kadir, D.H. & Hassanvand, A. Assessing the impact of aneurysm morphology on the risk of internal carotid artery aneurysm rupture: A statistical and computational analysis of endovascular coiling. *Phys. Fluids* **35**(10) (2023).
41. Zhou, L., Kadir, D. H., Shi, L., Mousavi, S. V., & Huang, X. The influence of aneurysm feature on coiling treatment of internal carotid artery aneurysms: Numerical and statistical study. *Int. J. Mod. Phys. C* 2450031 (2023).
42. Yang, J. & Kadir, D.H. Data mining techniques in breast cancer diagnosis at the cellular–molecular level. *J. Cancer Res. Clin. Oncol.* 1–16 (2023).
43. Ansys, I. "ANSYS® Fluent User's Guide, Release 2020 R2. Canonsburg: ANSYS." (2020).
44. Sadeghi, A., Amini, Y., Saidi, M. H. & Yavari, H. Shear-rate-dependent rheology effects on mass transport and surface reactions in biomicrofluidic devices. *AIChE J.* **61**(6), 1912–1924 (2015).
45. Zamani, M., Farahnakian, M. & Elhami, S. Employment of ultrasonic assisted turning in the fabrication of microtextures to improve the surface adhesion of the titanium implant. *Proc. Inst. Mech. Eng. Part B J. Eng. Manuf.* **235**(12), 1983–1991 (2021).
46. Khani, S., Haghighi, S.S., Razfar, M.R.& Farahnakian, M. Optimization of dimensional accuracy in threading process using solid-lubricant embedded textured tools. *Mater. Manuf. Process.* **37**(3), 294–304 (2021).
47. Sheidani, A., Salavatidezfouli, S. & Schito, P. Study on the effect of raindrops on the dynamic stall of a NACA-0012 airfoil. *J Braz. Soc. Mech. Sci. Eng.* **44**, 203. https://doi.org/10.1007/s40430-022-03498-8 (2022).
48. Sheidani, A., Salavatidezfouli, S., Stabile, G. & Rozza, G. Assessment of URANS and LES methods in predicting wake shed behind a vertical axis wind turbine. *J. Wind Eng. Ind. Aerodyn.* **232**, 105285 (2023).
49. Sheidani, A., Salavatidezfouli, S., Stabile, G., Gerdroodbary, M. B. & Rozza, G. Assessment of icing effects on the wake shed behind a vertical axis wind turbine. *Phys. Fluids 35*(9) *(2023).*

Author contributions

M.F. and S.A.A. wrote the main manuscript text and A.H.A and S.H. prepared figures and P.D. supervised the project. All authors reviewed the manuscript.

Competing interests

The authors declare no competing interests.

Additional information

Correspondence and requests for materials should be addressed to S.A.A. or S.H.

Reprints and permissions information is available at www.nature.com/reprints.

Publisher's note Springer Nature remains neutral with regard to jurisdictional claims in published maps and institutional affiliations.